Microchimica Acta (2019) 186: 294
https://doi.org/10.1007/s00604-019-3398-5

ORIGINAL PAPER

A FRET-based fluorescent probe for hydrogen peroxide based on the use of carbon quantum dots conjugated to gold nanoclusters

Qi Zhao[1] · Chaohui Zhou[1] · Qingye Yang[1] · Zhongyun Chu[1] · Nengqin Jia[1]

Received: 7 November 2018 / Accepted: 1 April 2019 / Published online: 23 April 2019

Abstract

In the Fenton reaction, ferrous ion acts as a catalyst and reacts with hydrogen peroxide (H_2O_2) to produce hydroxy radicals (·OH) and hydroperoxy radicals (·OOH). Both have much stronger oxidization ability than H_2O_2. A fluorescent probe for H_2O_2 is described here that was obtained by covalent conjugation of carbon quantum dots to gold nanoclusters (AuNCs). The conjugate, under 360 nm photoexcitation, displays dual (blue and red) emission, with peaks located at 450 and 640 nm. When introducing ·OH radicals via the Fenton reaction, the fluorescence intensities of both the CQDs and the AuNCs are decreased. The ratio of the fluorescence at the two peaks is related to the concentration of H_2O_2 in the 1.25 nM to 10 μM concentration range, and the detection limit is 0.16 nM. The probe was applied to the determination of H_2O_2 in milk and toothpaste and to cell imaging.

Keywords Dual-emission fluorescent probe · Fenton reaction · Hydrogen peroxide (H_2O_2) · Cellular imaging · Fluorescence resonance energy transfer · Ratiometric probe

Introduction

Hydrogen peroxide plays an important role in human health and life. Some pathogenic processes, such as ischemia-reperfusion injury, inflammation, carcinogenesis, and signal transduction are associated with the unintentional intake of H_2O_2 [1, 2]. Except for that, H_2O_2 is involved in food, industrial and environmental analyses and regarded as a carcinogen [3, 4]. Thus, there is a growing concern for developing simple, low-cost, and sensitive methods for determiation of H_2O_2 at trace levels.

Various analytical techniques such as phosphorescence spectrum, titration, chromatography and electrochemical have been put into H_2O_2 sensing [5–7]. Obviously, these approaches are influential thanks to high efficiency and selectivity, which have improved the advances of H_2O_2 sensing. In the past few years, fluorescence technology is one of the most exciting analysis methods based on its high sensitivity, admirable spatial/temporal resolution and convenient experiment operation [8, 9]. Although a vast amount of fluorescence probes have been explored, low stability due to autoxidation, photobleaching still a problem to be solved. Poor stability influenced by the environment is adverse for biological application as well.

Emerging nanotechnology and ratiometric sensing designs may provide a solution to these problems. In the first place, nanoparticles have been greatly developed as sensors agent for their intrinsic peculiarity [10, 11]. Among them, carbon quantum dots (CQDs) and noble metal nanoclusters have stayed in the frontline of analytical and cell imaging areas which based on their good water solubility, unique optical properties and low toxicity [12–15]. Gold nanoclusters (AuNCs) with the small diameter about 3 nm were aggregated of several metal atoms. Different from Au nanoparticles (AuNPs), AuNCs show no obvious surface plasmon resonance absorption while taking on luminescent in the region from the visible to NIR [16].

Electronic supplementary material The online version of this article (https://doi.org/10.1007/s00604-019-3398-5) contains supplementary material, which is available to authorized users.

✉ Nengqin Jia
nqjia@shnu.edu.cn

[1] The Education Ministry Key Laboratory of Resource Chemistry, Shanghai Key Laboratory of Rare Earth Functional Materials, and Shanghai Municipal Education Committee Key Laboratory of Molecular Imaging Probes and Sensors, College of Chemistry and Materials Science, Shanghai Normal University, 100 Guilin Road, Shanghai 200234, China

Secondly, ratiometric fluorescence sensors can output a more precise result than a single sensory unit that lack self-calibrating capabilities. This is because that certain ambiguities from environmental factors can be ruled out by the ratio of two-emission bands. Fluorescence resonance energy transfer (FRET) takes place when an excited state donor transfers energy to a ground state acceptor via dipole−dipole interactions [17], which can be seen as a special type of ratiometric fluorescence methods. In fact, there are continuing interest in developing a series of FRET sensors and have been widely applied in immunoassays interaction of biomacromolecules, and detection of small molecule [18, 19]. For example, Morteza's group fabricated an aptamer biosensor for monitoring aflatoxin B1 in peanut and rice sample [20]. Chang et al. have reported a FRET probe for ratiometric fluorescence Imaging of Iron in cells [21].

Herein, we introduced a novel FRET-based rational fluorescence probe for the detection of H_2O_2 in milk and toothpaste and efficient H_2O_2 imaging in vitro. The nanosized probe was named as nanoaster, and was constructed by branched poly(ethylenimine)-functioned carbon quantum dots (BPEI-CQDs) and gold nanoclusters synthesized with bovine serum albumin as a template (BSA@ AuNCs). Carbodiimide-activated coupling was linked reaction construction. Moreover, we applied Fenton reaction in our study, in which Fe^{2+} can react with hydrogen peroxide (H_2O_2) to form extremely reactive hydroxyl radicals (·OH) and hydroperoxyl radicals (·OOH). As a result, our proposed method contains the following remarkable features. First, the nano-biomaterials material was synthesized in a brief, convenient and bio-friendly route. Thus it is conducive for the further application. Next, ·OH produced by the Fenton reaction possesses the potential of 2.85 V which is much higher than H_2O_2 (1.776 V) [22], affording stronger oxidation capacity and higher sensitivity. Last but not least, the FRET-based ratiometric design will effectively eliminate the false positive signal, significantly heighten the accuracy of the result.

Experimental

Materials and methods

Lyophilized 99% bovine serum albumin (BSA), 1-ethyl-3-(3-dimethylaminopropyl carbodiimide (EDC), N-hydroxysuccinimide (NHS), Citric acid monohydrate, branched poly ethylenimine (M.W. 70,000, 99%), $HAuCl_4$ were purchased from Aladdin (Shanghai, China, http://www.aladdin-e.com/). Hydrogen peroxide, $FeSO_4.7H_2O$, $(NH_4)_2SO_4$ and other chemicals were obtained with Sinopharm Chemical Reagents Co. Ltd., (https://www.reagent.com.cn). Phorbol myristate acetate (PMA) was provided friendly by Bingxin Biotechnology Co. Ltd. The Michigan Cancer Foundation-7 cells (MCF-7) were purchased from the Chinese Academy of Science (http://www.cellbank.org.cn, Shanghai, China).

The morphology of the material was revealed with HRTEM (JEOL JEM-2100, http://www.jeol.co.jp/cn). Zeta potential and hydrodynamic diameter were measured with dynamic light scattering (MALVERN Nano ZS90, https://www.malvernpanalytical.com.cn/). Fluorescence spectrum was recorded with Ailgent Technologies Cary Eclipse Fluorescence Spectrophotometer (https://www.agilent.com/), UV-visible absorption spectra was detected on a Hitachi U-3900 UV/VIS spectrophotometer (Hitachi, Japan, http://www.hitachi-hightech.com). X-ray photoelectron spectroscopy (XPS, Perkin-Elmer PHI 5000C ESCA, https://www.perkinelmer.com.cn/) was to reflect the surface element composition. Fourier transforms infrared (FTIR) spectra of dried samples was acquired by a Nicolet 380 spectrometer, https://www.thermofisher.com/cn/zh/home.html. Metal concentration of the formed nanoparticles was measured by Varian 720-ES (ICP-AES), (https://www.agilent.com/).

Synthesis of dually emitting nanoclusters (CQD AuNCs)

According to the report [23, 24], the synthetic route of BPEI-CQDs and BSA@AuNCs were described in the Electronic Supporting Material in detail. Carbodiimide chemistry was introduced to conjugate BPEI-CQDs and BSA@AuNCs. Typically, 4 mL BSA@AuNCs and 10 $mg.mL^{-1}$ EDC/NHS were mixed in 50 mL beaker, and 4 mL 3 $mg.mL^{-1}$ BPEI-CQDs were added after 20 min later. The reaction was then allowed to proceed for 18 h at room temperature. At last, the final CQD-AuNCs nanoaster were extensively dialyzed (M.W. 3500) to remove unreacted reagents, and then freeze-drying to get pale yellow solid.

Fluorometric determination of H_2O_2

50 μL CQD-AuNCs nanoaster solution was diluted by 930 μL tris-HCl, and then 10 μL Fe^{2+} (40 mM) was induced for producing radical species. Subsequently, 10 μL of H_2O_2 with different concentrations were added to the above solution and collected the fluorescence emission spectra as photoexcited with 360 nm.

Analysis of real samples

The milk and toothpaste were bought from a local supermarket. Milk was diluted with water (1:3) and toothpaste was dissolved as 10 $mg.mL^{-1}$, firstly. 1.718 g $(NH_4)_2SO_4$ was added to the toothpaste solution. Then, the milk and toothpaste were centrifuged 15 min, at 8000 rpm, 4 °C and filtrated with 0.22 μm filter before used.

Intracellular imaging of H_2O_2

MCF-7 cells were seeded into confocal petri dish containing 90% DMEM and 10% FBS and allowed to culture for 12 h at 37 °C in a 5% CO 2 incubator. Then, washing the cells three times with DMEM and incubated CQD-AuNCs nanoaster for 5 h, followed by PMA (5 μg mL^{-1}) treatment for 0.5 h. Lastly, the intracellular imaging were recorded with fresh DMEM by Leica TCS SP5 II confocal laser scanning microscopy.

Results and discussion

Design strategy

Scheme 1 declares the designed course and the theory for H_2O_2 detection. In the program, BPEI-CQDs (donor) and BSA@AuNCs (acceptor) are linked by amido reaction, forming CQD-AuNCs nanoaster. Explicitly, when H_2O_2 is absent, the nanoaster displays a pink fluorescent colour which is the hybrid color of red-emitting AuNCs and blue-emitting CQDs. After introducing enough H_2O_2, the ·OH produced from the Fenton reaction will decrease the fluorescence intensity of CQD-AuNCs nanoaster with effect. Therefore, the established nanoprobe can be apply in detecting H_2O_2 appropriately.

Probe characterization and analysis

According to this idea, BPEI-CQDs and BSA@AuNCs were evolved, firstly. As exhibited in Fig. 1a, BPEI-CQDs showed the diameter of 2–3 nm in the TEM image. The CQDs possesses the maximum excitation wavelength at 360 nm (see Fig. S1) and a significant emission peak close to 450 nm that can be seen from Fig. 1b. At the same time, a bright blue color is easily catched from pellucid BPEI-CQDs solution when illuminated with UV lamp (Fig. 1c), confirming the successful synthesis of the fluorescent carbon quantum dots. Correspondingly, HRTEM image shows a monodisperse spherical morphology BSA@AuNCs with an average diameter about 3–5 nm in Fig. 1d. The EDS analysis of AuNCs appeas in Fig. S2, indicating the existence of Au in the particles. And, the fluorescence emission spectra of pale yellow-BSA@AuNC solution exhibits a maximum peak at 640 nm which was agreed with the red-emitting under the illumination of hand-held UV lamp (Fig. 1e and f). For the study, it was of interest to investigate the relationship between the fluorescence emission intensity of BSA@AuNCs and the reaction time. To our delight, there is a brighter fluorescence seen in Fig. S3 (Supporting Information) after extending the incubation time to 24 h. As described by Dynamic Light Scatting (DLS) in Fig. S4, the CQD-AuNCs nanoaster has a small diameter, approximately 8.097 nm. Furthermore, the diameter of BPEI-CQDs, BSA@AuNCs and CQD-AuNCs mixture (which combined using mechanical stirring) are about 1.856 nm, 2.434 nm and 96.992 nm, respectively. Thus, compared to individual CQDs and AuNCs, the slight increase in hydrodynamic diameter of CQD-AuNCs nanoaster proves the coupling of nanoaster in a way. Moreover, the four materials prepared above can be characterized by zeta potential test. As depicted in Fig. S5, the potential of BPEI-CQDs is positive which can be ascribed to abundant amine groups exposed on the surface of CQDs. The zeta potential of nanomixture falls between CQDs and AuNCs, which can be explained by the interaction of electrostatic attraction. In addition, Fourier transform infrared (FTIR) analysis of Fig. 1g was further carried out to verify the attachment of CQDs and AuNCs by identifying organic functional groups. Clear to see, CQDs appears two bands at 3246 cm^{-1} and 1589 cm^{-1}, probably owing to the stretching and bending vibrations of N-H [23]. Three peaks at 3227 cm^{-1}, 2960 cm^{-1}, 1650 cm^{-1} of BSA@AuNCs are attributed to the N-H, C–H and C=O

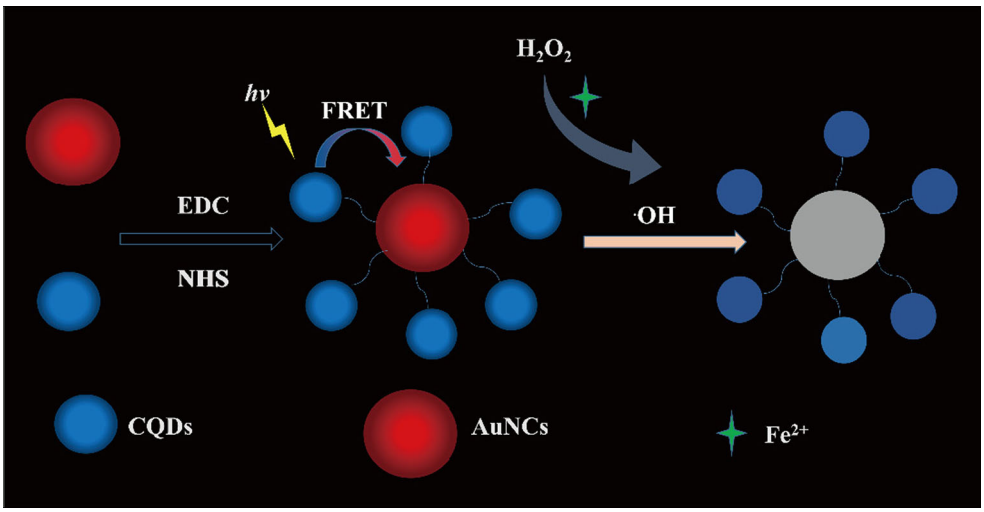

Scheme 1 Schematic representation of a FRET-based fluorescent probe and enhanced performance of hydrogen peroxide by Fenton reaction. The fluorescence intensity of CQD-AuNCs nanoaster was decreased as introducing H_2O_2 to the probe, and can be applied to the determination of milk and toothpaste and cells imaging

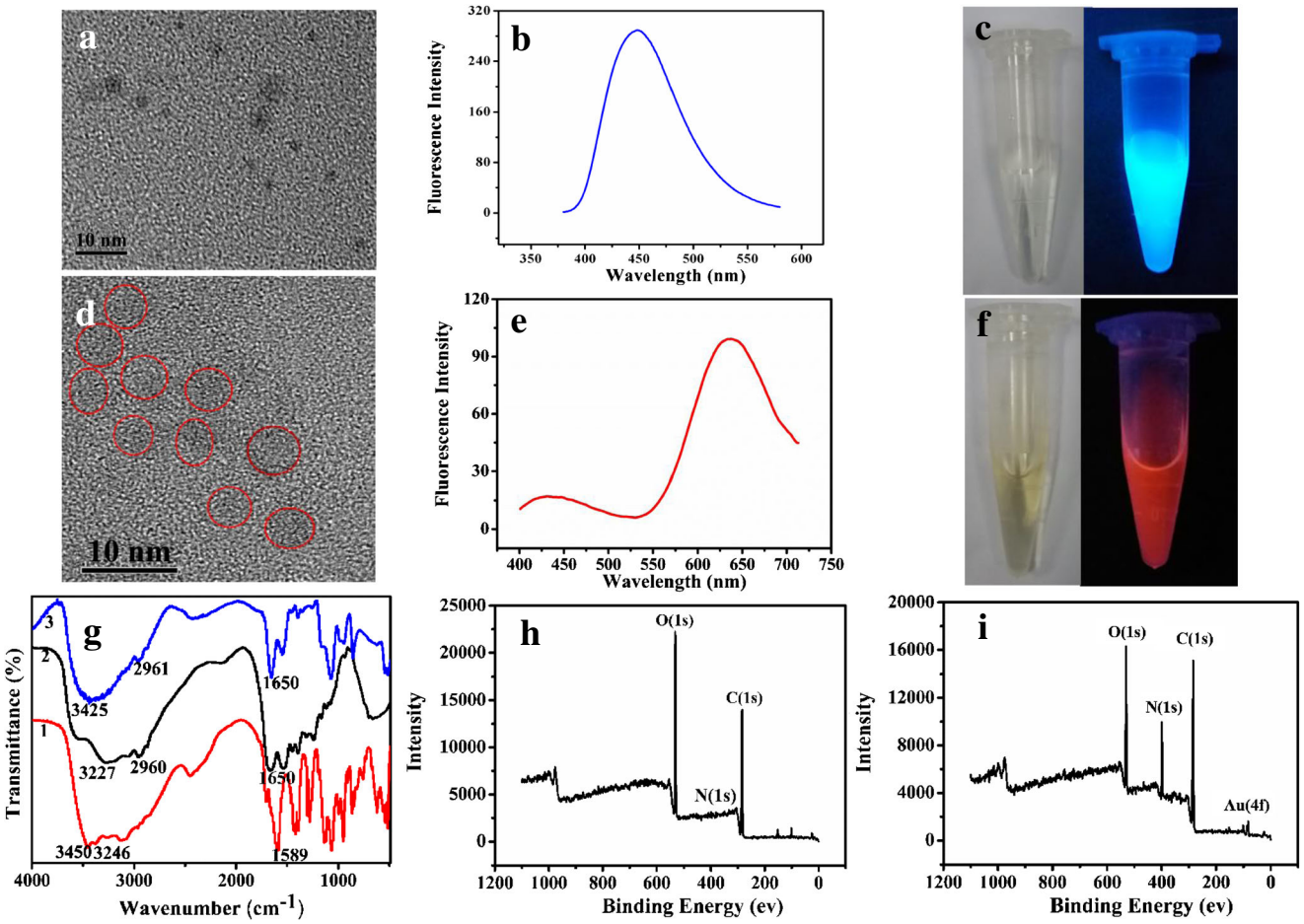

Fig. 1 TEM image (1**a**) and fluorescence plot (1**b**) of the BPEI-CQDs; Photographs of CQDs (1**c**) under (left) visible and (right) UV light; TEM picture (1**d**) and fluorescence plot (1**e**) of the BSA@AuNCs; Photographs of BSA@AuNCs (1**f**) under (left) visible and (right) UV light; 1**g**: FT-IR spectra of the BPEI-CQDs (1), BSA@AuNCs (2), CQD-AuNCs nanoaster (3); X-ray photoelectron spectroscopy spectra of the BPEI-CQDs (1**h**) and CQD-AuNCs nanoaster (1**i**)

stretching vibrations. Noticing that, the characteristic peaks of 3425 cm^{-1}, 2961 cm^{-1}, 1650 cm^{-1} in the nanoaster demonstrate many amino, hydroxyl and carbonyl groups coving the surfaces of nanoparticles. Therefore, successful polymerization of the nanomaterial driven by acylamide bonds can be partially demonstrates. The surface element analysis was determined by X-ray photoelectron spectroscopy. As expressed in Fig. 1h and i, the CQD-AuNCs nanoaster own extra gold peak compared to BPEI-CQDs. It provide an evidence that AuNCs was joint to the CQDs as well. The bonding form in the high-resolution XPS spectra of C1s and O1s spectra (Fig. S6) also corresponding to FT-IR.

All of these above assays confirmed the successful preparation and modification of CQD-AuNCs nanoaster. And now, it is time to make a thorough inquiry in its fluorescence properties. It is apparent that the fluorescence intensity at 650 nm of CQD-AuNCs nanoaster was enhanced and had a red shift in comparison to the BSA@AuNCs (640 nm). Simultaneously, the intensity at 450 nm is decreased tremendously than BPEI-CQDs (Fig. 2a). But, CQD-AuNCs nanomixture formed by direct mixing of BPEI-CQDs and BSA@AuNCs did not exhibit such properties. This phenomenon may be stemmed from energy transfer between BPEI-CQDs (donor) and BSA@AuNCs (acceptor), theraby enhancing the fluorescence intensity of AuNCs. Consequently, we guess that the use of nanoaster as a probe may result in a higher sensitivity and lower detection limits. And, the fluorescence lifetime of CQDs is decreased after conjugating with AuNCs. (Seen in Fig. S7). Besides, BSA@AuNCs presents three excitation peaks that are loaded around 308, 365, 470 nm. In Fig. 2b, an appreciably overlap in the range of 400–550 nm between the fluorescence emission spectra from BPEI-CQDs and

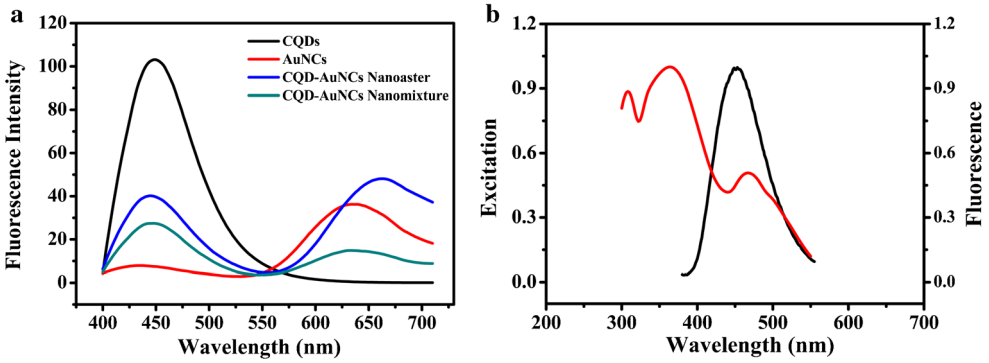

Fig. 2 **a:** The spectra of fluorescence emission that BPEI-CQDs (black), BSA@AuNCs (red), CQD-AuNCs nanoaster (blue) and CQD-AuNCs nanomixture (green); **b**: The overlapping plot of emission spectra of BPEI-CQDs (black) and excitation spectra of BSA@AuNCs (red)

excitation spectra of BSA@AuNCs, certifying the possibility of FRET to some extent. Contacting with the previous explanation about hydrodynamic diameters of BPEI-CQDs, BSA@AuNCs and CQD-AuNCs, the size growth of nanoaster is less than 10 nm, which is also match the condition of resonance energy transfer.

Fluorometric determination of H_2O_2

For obtaining the best result, several factors need to be taken into account, including pH and incubation time (Fig. S8). According to the data and the proper physiological environment, we thought pH = 7 and 30 min of incubation time are

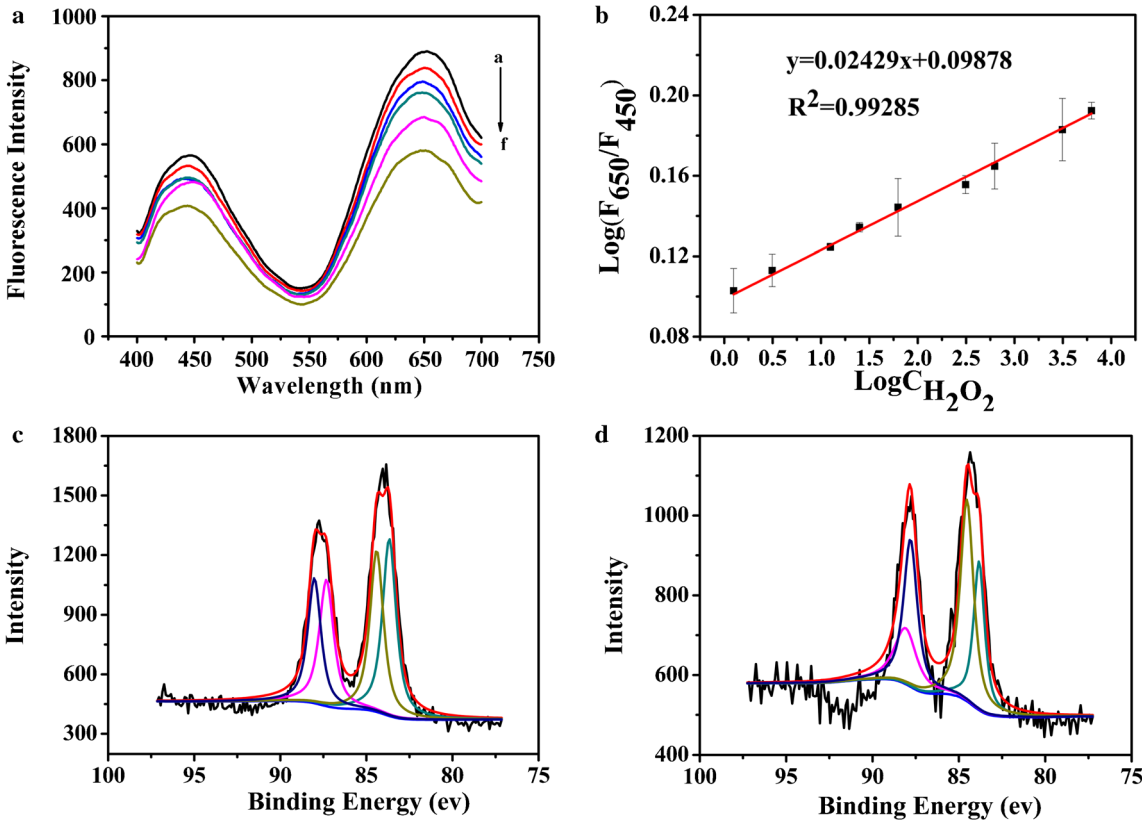

Fig. 3 **a**: Fluorescence spectra of CQD-AuNCs nanoaster with different concentration of H_2O_2 (a-f: 0, 10^{-9}, 10^{-8}, 10^{-7}, 10^{-5}, 10^{-4} M); **b**: Ratiometric fluorescence as the logarithmic function to the H_2O_2 concentration; High-resolution Au 4f peaks of CQD-AuNCs nanoaster in the absence (**c**) and presence (**d**) of 1.0 mM H_2O_2

proper for the experiment. Thus, the fluorescence response of CQD-AuNCs nanoaster toward H_2O_2 was further evaluated under physiological condition. Figure 3a represents the fluorescence changes of CQD-AuNCs upon addition of ·OH. Here, Fe^{2+} is excessive and served as the catalyst to produce ·OH during the reaction with H_2O_2. As the H_2O_2 concentration increased from 0.00125 to 10 μM, the nanoaster showed substantially quenching fluorescence at 450 nm and 650 nm. Interestingly, as the amount of H_2O_2 increased, the fluorescence intensity ratio (F_{650} nm/F_{450} nm) changed continuously and the linear relationship between the logarithmic function of F_{650}/F_{450} nm value and H_2O_2 concentration was exhibited. (Seen in the Fig. 3b) The corresponding lineal relation can be described as $Y = 0.2429X + 0.09878$ ($R^2 = 0.99285$), in which Y is the logarithmic of the fluorescence intensity ratio, and X represents the logarithmic of concentration from H_2O_2. The limit of detection of 1.59 nM was gained, that is much lower than previously reported probes [25–29]. There is a clear comparison made in the Table 1. The selectivity of the sensing system toward H_2O_2 supported by Fenton reaction was assessed by using 10-fold H_2O_2, different amino acids and Cu^{2+}, NO_2^- as contrast. As shown in Fig. S9, the test method has a distinct effect on H_2O_2 under the identical conditions. A real sample experiment of milk and toothpaste was performed and the results are recorded on the Table S1 (Electronic Supporting Material). It was no found in the real samples and the spiked recoveries and relative standard deviation are keept in a satisfactory range.

The mechanism of H_2O_2 sensing

To speculate the reason for fluorescence quenching, the XPS spectra that CQD-AuNCs nanoaster with H_2O_2 was studied in the next step. The XPS spectra of the CQD-AuNCs nanoaster in the Au $4f_{7/2}$ is divided into two parts: 83.65 ev [Au (0)] and 84.45 ev [Au (I)], which has good accordance with the previous literature [32, 33]. By comparison Fig. 3c and d, the proportion of Au (I) in the AuNCs increased saliently after the introduction of H_2O_2, indicating that AuNCs was oxidized by ·OH. On the other hand, the fluorescence intensity of BPEI-CQDs shows little change (<5%) with increasing concentration of H_2O_2, indicating that there is no interaction between BPEI-CQDs and H_2O_2 (Fig. S10A). In summary, the possible reason for fluorescence quenching of the nanoaster is assigned to the powerful oxidation ability of ·OH [34] What's more, the variation of absorption spectrum have been paid to explore measurement mechanism of the assay. Comparing with three absorption bands in Fig. S10B, it is easy to find that an increase in the absorption intensity of AuNCs, which may cause a decrease in the fluorescence intensity of CQDs. The reason may be that more energy from CQDs is absorbed and transferred to AuNCs. Hence, we can conclude that the oxidation of AuNCs and the energy transformation between CQD and AuNCs induce efficient fluorescence quenching of the sensing system.

Cytotoxicity and intracellular imaging

To investigate whether the probe can be applied to biological systems or not, the cytotoxicity of material was first evaluated. As demonstrated in Fig. S11, over 94% cell survival rate can be reached after the MCF-7 cells incubating with 45.66 μg mL^{-1} nanoaster for 24 h.

Then the ability of intracellular imaging was further explored. As revealed in Fig. 4, there is a visible fluorescence in the cells when cells were incubation with nanoaster for 12 h, which indicates a satisfactory cell permeability. Followed previous report [35], we added PMA and Fe^{2+} to produce ·OH in the cell. It was evident that the fluorescence

Table 1 Comparison of different sensors for the detection of H_2O_2

Method	Sensors	Linear range	LOD (μM)	Ref
Electrochemical	AgNPs/p-isopropyl calix [6] arene/modified GC electrode	0.05–6.5 mM	27	[25]
Electrochemical	Polyethyleneimine-templated silver nanoclusters modified GC electrode (PEI/AgNCs–GCE)	10–1440 μM	1.8	[26]
Electrochemical	Flower-like Bi_2Se_3 nanostructures/hemoglobin/modified GC electrode	2–100 μM	0.63	[27]
Electrochemical	3D nanoporous Ag@BSA composite microspheres	5 μM–1.5 mM	0.16	[30]
Fluorescence	glucose oxidase–stabilized gold nanoclusters	0.5-10 μM	0.23	[31]
Fluorescence	Polyethyleneimine-capped silver nanoclusters (PEI-Ag NCs)	0.5–100 μM	0.40	[28]
Fluorescence	Three-dimensional Fe- and N-incorporated carbon structures	0.1–100 μM	0.068	[29]
Fluorescence	CQD-AuNCs	0.00125–10 μM	0.000159	This work

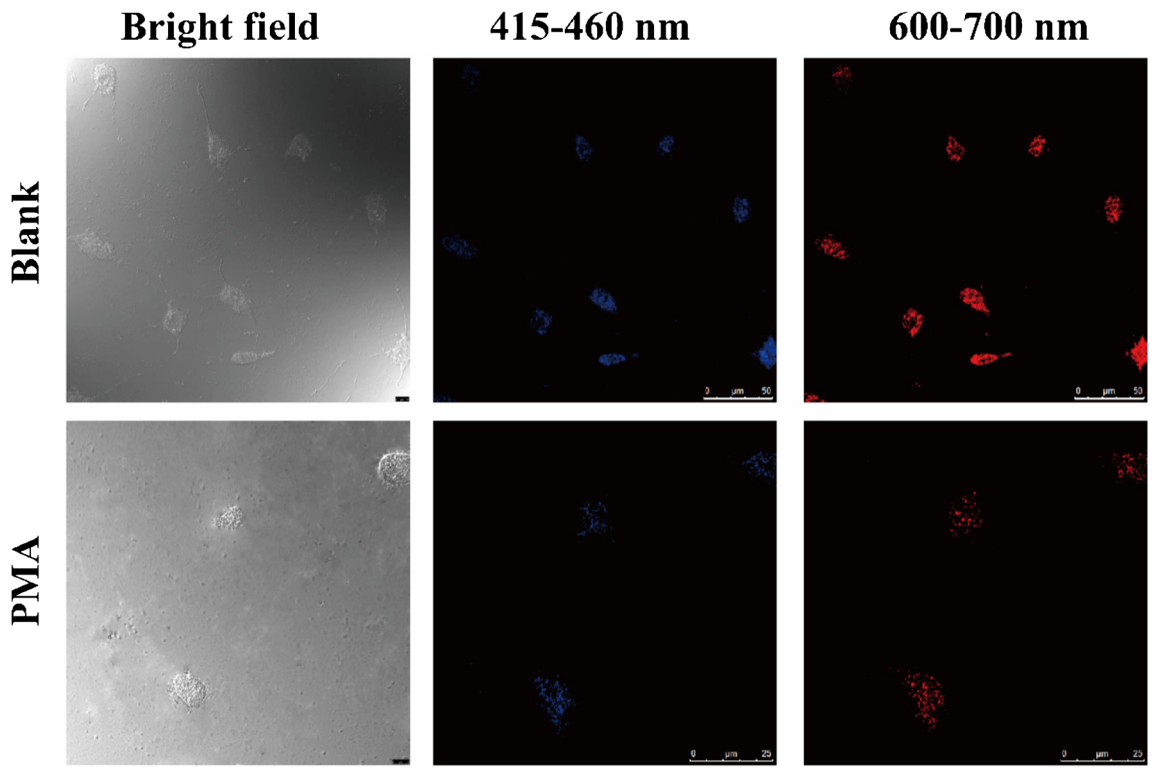

Fig. 4 Fluorescence imaging images of bright-field and different wavelengths of CQD-AuNCs nanoaster cells were incubated without (top) and without (bottom) PMA stimulation. Scale scale is 10 μm

signal was relatively weak in both channels of 415–460 nm and 600–700 nm, which has the similar phenomenon to the vitro experiment. In general, it was suitable to apply the nanoprobe in live cell imaging by the bright fluorescence performance.

Conclusions

We have developed a new fluorescent probe for highly sensitive detection of H_2O_2, which is constructed by amide interaction between amino-functional CQDs and AuNCs modified by carboxyl groups. The CQD-AuNCs nanoaster embodies dual emission bands as excited under a single wavelength and occurs energy resonance transfer, resulting in high sensitivity and selectivity. The use of a ratiometric probe can eliminate environmental influence and improve accuracy. Additionally, the study presents a method for H_2O_2 determination in milk and toothpast and imaging in live cells. Sincerely, we hope that this experiment may provide a thought or method and pave the road for further exploration in future. Such long wavelength probes are preferred when application in the vivo for reducing biological interferences.

Acknowledgments We thank financially support from Shanghai Science and Technology Committee (17070503000), Shanghai Engineering Research Center of Green Energy Chemical Engineering, International Joint Laboratory on Resource Chemistry (IJLRC), Program for Changjiang Scholars and Innovative Research Team in University (IRT_16R49).

Author contributions The manuscript was written through contributions of all authors. All authors have given approval to the final version of the manuscript.

Compliance with ethical standards The author(s) declare that they have no competing interests.

References

1. Li S, Chang K, Sun K, Tang Y, Cui N, Wang Y, Qin W, Xu H, Wu C (2016) Amplified singlet oxygen generation in semiconductor polymer dots for photodynamic Cancer therapy. ACS Appl Mater Interfaces 8:3624–3634
2. Sheng J, Jiang X, Wang L, Yang M, Liu YN (2018) Biomimetic mineralization guided one-pot preparation of gold clusters anchored two-dimensional MnO_2 Nanosheets for Fluorometric/magnetic bimodal sensing. Anal Chem 90:2926–2932

3. Liu B, Sun Z, Huang PJ, Liu J (2015) Hydrogen peroxide displacing DNA from Nanoceria: mechanism and detection of glucose in serum. J Am Chem Soc 137:1290–1295
4. Sadhukhan M, Bhowmik T, Kundu MK, Barman S (2014) Facile synthesis of carbon quantum dots and thin graphene sheets for non-enzymatic sensing of hydrogen peroxide. RSC Adv 4:4998
5. Bai J, Jiang X (2013) A facile one-pot synthesis of copper sulfide-decorated reduced graphene oxide composites for enhanced detecting of H2O2 in biological environments. Anal Chem 85:8095–8101
6. Chen W, Cai S, Ren QQ, Wen W, Zhao YD (2012) Recent advances in electrochemical sensing for hydrogen peroxide: a review. Analyst 137:49–58
7. Guler M, Turkoglu V, Kivrak A, Karahan F (2018) A novel non-enzymatic hydrogen peroxide amperometric sensor based on Pd@CeO_2-NH_2 nanocomposites modified glassy carbon electrode. Mater Sci Eng C 90:454–460
8. Bag N, Wohland T (2014) Imaging fluorescence fluctuation spectroscopy: new tools for quantitative bioimaging. Annu Rev Phys Chem 65:225–248
9. Koike S, Kawamura K, Kimura Y, Shibuya N, Kimura H, Ogasawara Y (2017) Analysis of endogenous H_2S and H_2Sn in mouse brain by high-performance liquid chromatography with fluorescence and tandem mass spectrometric detection. Free Radic Biol Med 113:355–362
10. Han GM, Li H, Huang XX, Kong DM (2016) Simple synthesis of carboxyl-functionalized upconversion nanoparticles for biosensing and bioimaging applications. Talanta 147:207–212
11. Yang DP, Guo W, Cai Z, Chen Y, He X, Huang C, Zhuang J, Jia N (2018) Highly sensitive electrochemiluminescence biosensor for cholesterol detection based on AgNPs-BSA-MnO_2 nanosheets with superior biocompatibility and synergistic catalytic activity. Sensors Actuators B Chem 260:642–649
12. Peng Z, Miyanji EH, Zhou Y, Pardo J, Hettiarachchi SD, Li S, Blackwelder PL, Skromne I, Leblanc RM (2017) Carbon dots: promising biomaterials for bone-specific imaging and drug delivery. Nanoscale 9:17533–17543
13. He W, Gui R, Jin H, Wang B, Bu X, Fu Y (2018) Ratiometric fluorescence and visual imaging detection of dopamine based on carbon dots/copper nanoclusters dual-emitting nanohybrids. Talanta 178:109–115
14. Gao J, Li Q, Wang C, Tan H (2017) Copper (II)-mediated fluorescence of lanthanide coordination polymers doped with carbon dots for ratiometric detection of hydrogen sulfide. Sensors Actuators B Chem 253:27–33
15. Zhou R, Li Y, Tian Y, Sun Q, Deng P, Wu L, Hou X (2017) Simple fluorescence sensing of extreme acidity based on inner filter effect of ascorbic acid to fluorescent Au nanoclusters. Nanoscale 9:10167–10172
16. Zheng J, Zhou C, Yu M, Liu J (2012) Different sized luminescent gold nanoparticles. Nanoscale 4:4073–4083
17. Chen G, Song F, Xiong X, Peng X (2013) Fluorescent nanosensors based on fluorescence resonance energy transfer (FRET). Ind Eng Chem Res 52:11228–11245
18. Jin B, Wang S, Lin M, Jin Y, Zhang S, Cui X, Gong Y, Li A, Xu F, Lu TJ (2017) Upconversion nanoparticles based FRET aptasensor for rapid and ultrasenstive bacteria detection. Biosens Bioelectron 90:525–533
19. Claussen JC, Algar WR, Hildebrandt N, Susumu K, Ancona MG, Medintz IL (2013) Biophotonic logic devices based on quantum dots and temporally-staggered Forster energy transfer relays. Nanoscale 5:12156–12170
20. Sabet FS, Hosseini M, Khabbaz H, Dadmehr M, Ganjali MR (2017) FRET-based aptamer biosensor for selective and sensitive detection of aflatoxin B1 in peanut and rice. Food Chem 220:527–532
21. Aron AT, Loehr MO, Bogena J, Chang CJ (2016) An Endoperoxide reactivity-based FRET probe for Ratiometric fluorescence imaging of labile Iron pools in living cells. J Am Chem Soc 138:14338–14346
22. Zong C, Wang M, Li B, Liu X, Zhao W, Zhang Q, Liang A, Yu Y (2017) Sensing of hydrogen peroxide and glucose in human serum via quenching fluorescence of biomolecule-stabilized Au nanoclusters assisted by the Fenton reaction. RSC Adv 7:26559–26565
23. Dong Y, Wang R, Li G, Chen C, Chi Y, Chen G (2012) Polyamine-functionalized carbon quantum dots as fluorescent probes for selective and sensitive detection of copper ions. Anal Chem 84:6220–6224
24. Xie JP, Zheng Y, Ying JY (2009) Protein-directed synthesis of highly fluorescent gold nanoclusters. J Am Chem Soc 131:888–889
25. Raoof JB, Ojani R, Hasheminejad E, Rashid-Nadimi S (2012) Electrochemical synthesis of Ag nanoparticles supported on glassy carbon electrode by means of p-isopropyl calix[6]arene matrix and its application for electrocatalytic reduction of H_2O_2. Appl Surf Sci 258:2788–2795
26. Li BL, Chen JR, Luo HQ, Li NB (2013) Electrocatalytic activity of polymer-stabilized silver nanoclusters for hydrogen peroxide reduction. J Electroanal Chem 706:64–68
27. Fan H, Zhang S, Ju P, Su H, Ai S (2012) Flower-like Bi_2Se_3 nanostructures: synthesis and their application for the direct electrochemistry of hemoglobin and H_2O_2 detection. Electrochim Acta 64:171–176
28. Wen T, Qu F, Li NB, Luo HQ (2012) Polyethyleneimine-capped silver nanoclusters as a fluorescence probe for sensitive detection of hydrogen peroxide and glucose. Anal Chim Acta 749:56–62
29. Zhang R, He S, Zhang C, Chen W (2015) Three-dimensional Fe- and N-incorporated carbon structures as peroxidase mimics for fluorescence detection of hydrogen peroxide and glucose. J Mater Chem B 3:4146–4154
30. Liu Q, Zhang T, Yu L, Jia N, Yang DP (2013) 3D nanoporous Ag@BSA composite microspheres as hydrogen peroxide sensors. Analyst 138:5559–5562
31. Cui W, Qin H, Zhou Y, Du J (2017) Determination of the activity of hydrogen peroxide scavenging by using blue-emitting glucose oxidase-stabilized gold nanoclusters as fluorescent nanoprobes and a Fenton reaction that induces fluorescence quenching. Microchim Acta 184:1103–1108
32. Jin L, Shang L, Guo S, Fang Y, Wen D, Wang L, Yin J, Dong S (2011) Biomolecule-stabilized Au nanoclusters as a fluorescence probe for sensitive detection of glucose. Biosens Bioelectron 26:1965–1969
33. Dasog M, Scott RWJ (2007) Understanding the oxidative stability of gold monolayer-protected clusters in the presence of halide ions under ambient conditions. Langmuir 23:3381–3387
34. Masanta G, Heo CH, Lim CS, Bae SK, Cho BR, Kim HM (2012) A mitochondria-localized two-photon fluorescent probe for ratiometric imaging of hydrogen peroxide in live tissue. Chem Commun 48:3518
35. Ju E, Liu Z, Du Y, Tao Y, Ren J, Qu X (2014) Heterogeneous assembled Nanocomplexes for Ratiometric detection of highly reactive oxygen species in vitro and in vivo. ACS Nano 8:6014–6023